HHS Public Access

Author manuscript

Microvasc Res. Author manuscript; available in PMC 2022 November 01.

Published in final edited form as:

Microvasc Res. 2021 November ; 138: 104205. doi:10.1016/j.mvr.2021.104205.

Morphological characterization of *Etv2* vascular explants using fractal analysis and atomic force microscopy

Robert P. Adelson[a], **Brisa Palikuqi**[b], **Zachary Weiss**[a], **Antonio Checco**[a], **Ryan Schreiner**[c], **Shahin Rafii**[b], **Sina Y. Rabbany**[a,b,*]

[a]Bioengineering Program, DeMatteis School of Engineering and Applied Science, Hofstra University, Hempstead, NY, USA.

[b]Division of Regenerative Medicine, Ansary Stem Cell Institute, Department of Medicine, Weill Cornell Medicine, New York, NY, USA.

[c]Department of Ophthalmology, Margaret Dyson Vision Research Institute, Weill Cornell Medicine, New York, NY, USA.

Abstract

The rapid engraftment of vascular networks is critical for functional incorporation of tissue explants. However, existing methods for inducing angiogenesis utilize approaches that yield vasculature with poor temporal stability or inadequate mechanical integrity, which reduce their robustness in vivo. The transcription factor Ets variant 2 (Etv2) specifies embryonic hematopoietic and vascular endothelial cell (EC) development, and is transiently reactivated during postnatal vascular regeneration and tumor angiogenesis. This study investigates the role for *Etv2* upregulation in forming stable vascular beds both *in vitro* and *in vivo*. Control and *Etv2*$^+$ prototypical fetal-derived human umbilical vein ECs (HUVECs) and adult ECs were angiogenically grown into vascular beds. These vessel beds were characterized using fractal dimension and lacunarity, to quantify their branching complexity and space-filling homogeneity, respectively. Atomic force microscopy (AFM) was used to explore whether greater complexity and homogeneity lead to more mechanically stable vessels. Additionally, markers of EC integrity were used to probe for mechanistic clues. *Etv2*$^+$ HUVECs exhibit greater branching, vessel density, and structural homogeneity, and decreased stiffness *in vitro* and *in vivo*, indicating a greater propensity for stable vessel formation. When co-cultured with colon tumor organoid tissue, *Etv2*$^+$ HUVECs have decreased fractal dimension and lacunarity compared to *Etv2*$^+$ HUVECs cultured alone, indicating that vessel density and homogeneity of vessel spacing increased due to the presence of Etv2. This study sets forth the novel concept that fractal dimension, lacunarity, and AFM are as informative as conventional angiogenic measurements, including vessel branching and density, to assess vascular perfusion and stability.

*Corresponding Author: Sina Y. Rabbany, Bioengineering Program, DeMatteis School of Engineering and Applied Science, Hofstra University, Hempstead, NY 11549, United States, sina.y.rabbany@hofstra.edu.

Keywords

Fractal dimension; Lacunarity; Vascular engraftment; HUVECs; Adipose-derived endothelial cells; Ets variant 2; Angiogenesis; Atomic force microscopy; F-actin

Introduction

Cell and tissue explant transplantation faces a critical challenge due to a lack of strategies to ensure effective engraftment through the integration of vascular networks. The rapid engraftment of vascular networks is critical for functional incorporation of the transplanted cells (Palikuqi et al., 2020). However, existing methods for inducing angiogenesis utilize growth factors and biomaterials that do not satisfactorily yield vasculature with temporal stability or adequate mechanical integrity for reliable use *in vivo* (Kant and Coulombe, 2018; Mastrullo et al., 2020). We previously developed a strategy for rapid creation of vasculature and its subsequent introduction into transplanted tissue (Palikuqi et al., 2020), and identified the important future step of characterizing the morphology and stability of these vessel beds. Utilizing the foundations of vasculogenesis and angiogenesis found in embryonic growth is vital to enhance vessel morphological properties (Ding et al., 2020).

The vessel morphology present in adults depends on a multitude of genetic, systemic, and environmental factors. The extent and occurrence of the angiogenic process itself depends greatly on genetic and biomechanical control during development, remodeling due to the varying metabolic demands of tissues, and pathological events (Gould et al., 2011). A logical starting point to search for a factor to induce vessel growth in engrafted tissues is a developing embryo, where new vessel growth is rapid and dense. One essential transcription factor in hematopoietic and vascular development is Ets variant 2 (Etv2), with its encoding gene *Etv2* highly expressed in hemangioblasts compared to subsequently derived hematopoietic and endothelial cells. With *Etv2* silenced following initial generation of the hematopoietic and vascular systems, the gene is only transiently reactivated following injuries requiring vascular regeneration (Baltrunaite et al., 2017; Park et al., 2016; Singh et al., 2019; Zhao et al., 2017). Therefore, as a platform to uncover the contribution of mechanical and morphological properties that guide vascular formation, localized and systemic regulation of *Etv2* is an approach to design therapies for vascular deficiencies, cancer therapy, and tissue graft vascularization (Tanaka et al., 2018).

Therefore, it is necessary to quantify the mechanism by which *Etv2* upregulation augments angiogenic sprouting. Classical methods of measuring vessel growth, including mean density and mean diameter, are insufficient on their own for quantifying the success of vessel ingrowth, as they use Euclidean geometries (Essay and Maina, 2020; Gould et al., 2011; Plotnick et al., 1996). Vessel branching and space-filling exhibit a hierarchical self-similarity best quantified using non-Euclidean fractal mathematics, in particular the parameters of fractal dimension and lacunarity. Fractal dimension, a ratio indicating the change in complexity of a fractal pattern's details with scale, and lacunarity, a method of quantifying the size distribution of gaps between branches of a fractal pattern, are essential tools in fractal mathematics (Lennon et al., 2015; Wang et al., 2019). These two parameters,

we well as multifractal approaches, have been used to characterize human vasculature, most commonly retinal vessel networks (Ţălu, 2013; Ţălu, 2015). Additionally, vessel stability can be investigated using atomic force microscopy (AFM) to elucidate mechanical differences (such as stiffness) between *Etv2*$^{+}$ and control ECs and vessels (Frye et al., 2018; Palikuqi et al., 2020).

Magnifying a fractal pattern, such as that of a branching vessel, reveals additional details not resolvable at the original scale. Therefore, length is not a comprehensive measurement of scale on its own. Fractal dimension (D) is a more useful descriptor, allowing for the quantification of a vessel system's dimension, which lies between one and two dimensions when viewed as a plane, and between two and three dimensions when viewed using a three-dimensional modality (Mainster, 1990). A perfectly straight vessel with no branching has $D = 1$, a simple curved vessel with no branching has a D slightly greater than 1 (perhaps 1.1 or 1.2), and a vessel with significant branching and curvature may approach $D = 1.6$ to 1.8. The self-similarity of a fractal pattern is described by the formula

$$N_r = r^{-D} \tag{1}$$

where N_r is some measurement applied on the pattern at scale r, and D is the fractal dimension (Gadde et al., 2016). This can be rewritten by solving for D (Wang et al., 2019):

$$D = -\lim_{r \to 0} \frac{\log N_r}{\log r} \tag{2}$$

A classic example of a fractal curve is the Koch snowflake, which is recursively constructed and based upon the Koch curve described by Helge von Koch in 1904 (von Koch, 1904). This pattern begins with an equilateral triangle (Fig. 1a, iteration 1). The inner third of each side is then removed, and another equilateral triangle is built at the location where the side was removed (Fig. 1a, iteration 2). This process is repeated indefinitely (beginning with Fig. 1a, iteration 3) to construct an ever more complex fractal.

Lacunarity, a scale-dependent property, is the degree of deviation of any pattern from translational invariance (i.e., a measure of heterogeneity). In other terms, lacunarity describes the size and regular spacing of gaps among branches of a fractal pattern. Lacunarity is a dimensionless representation of the variance to mean ratio, equated by

$$\Lambda_{r,g} = \left(\frac{\sigma_{r,g}}{\mu_{r,g}}\right)^2 \tag{3}$$

where $\Lambda_{r,g}$ is lacunarity, $\sigma_{r,g}$ is the standard deviation of number of pixels per box, and $\mu_{r,g}$ is mean number of pixels per box, all at a given box size r and grid orientation g (Plotnick et al., 1996). It is important to note that as $\mu_{r,g}$ approaches zero, $\Lambda_{r,g}$ approaches infinity, with $\sigma_{r,g}$ being a constant. Therefore, a pattern with more gaps will have a higher lacunarity than a denser set, assuming the same box size r is used. Additionally, as r increases (larger boxes are used), lacunarity for the same pattern will decrease (Lennon et al., 2015; Plotnick et al., 1996; Zaia, 2015).

In addition to fractal analysis, investigation of the nanomechanical properties of the cells involved in angiogenesis is important to understand the effects of altering *Etv2* expression. AFM has become a widely accepted tool to study the mechanical properties of biological cells through indentation (Haase and Pelling, 2015). AFM provides an accurate method for characterization of elastic properties of soft, hydrated, and temperature-sensitive materials such as endothelial cells (ECs) (Dufrêne et al., 2017).

The first aim of the present study is to determine whether there is a correlation between non-Euclidean measures (fractal dimension and lacunarity) and *Etv2* upregulation and subsequent vessel stability in healthy colon and colon tumor. The second aim is to determine whether the fractal dimension and lacunarity can together be used as a reliable method to check vessel stability in the context of co-culture with healthy and tumor colon organoids. Using image processing and statistical methods, the various experimental and control vascular beds were treated as fractal geometries, and comparisons were made between healthy control and $Etv2^{+}$ human umbilical vein endothelial cells (HUVECs) and tumorigenic control and $Etv2^{+}$ cells. AFM was used to characterize the mechanical stiffness of normal and $Etv2^{+}$ HUVECs, necessary to correlate fractal properties with mechanical properties, thus bridging the gap between complex mathematics and clinical significance.

Materials and Methods

Cell culture

The following cell culture process was previously reported (Palikuqi et al., 2020). Approval for the use of discarded leftover HUVECs and human adipose tissue ECs, as well as normal and adenoma tissues collected from colonic resections, was obtained through the Weill Cornell Medicine Institutional Review Board (IRB). Prototypical fetal-derived HUVECs were isolated in the laboratory using collagenase as previously described (Zhang et al., 2003). The cells were then grown in tissue culture dishes coated with 0.2% gelatin and containing complete EC medium (400 ml M199, 100 ml heat-inactivated fetal bovine serum (FBS), 7.5 ml HEPES, 5 ml Penicillin/Streptomycin (Thermo Fisher Scientific, 15070063), 5 ml GlutaMAX (Thermo Fisher Scientific, 35050061), 5 ml of a lipid mixture (Thermo Fisher Scientific, 11905031), and 25 mg EC growth supplement (Alpha Aesar, J64516-MF)). The lipid mixture contained 95% human endothelial serum-free medium, 2% FBS, 15 mM HEPES, 50 μg/ml heparin, 1X antibiotic/antimycotic solution, 2 mM L-Glutamine, 250 ng/ml endothelial cell growth factor, and 250 ng/ml fibroblast growth factor. The cells were transduced with lenti-PGK-ETV2 or an empty lentiviral vector at passage 1–2 as we previously described (Palikuqi et al., 2020). ECs with or without *Etv2* were set in culture dishes and were treated after 24 hours with RAP1 inhibitor (GGTI-298, Tocris) resuspended in DMSO at a 1:1,000 dilution, while the same volume of DMSO was added to the control wells. Image stacks were obtained using a Zeiss 710 confocal microscope (Carl Zeiss Microscopy, Germany). This procedure was performed for control and $Etv2^{+}$ HUVECs alone, and $Etv2^{+}$ HUVECs in the presence of either normal colon or colon tumor organoids.

In vivo models

A previously described methodology for development and implantation of tissue plugs in mice was followed (Palikuqi et al., 2020). Approval for all animal experiments was obtained through the Weill Cornell Medicine Institutional Animal Care and Use Committee (IACUC). HUVECs and adipose-derived ECs were transduced with an empty lentiviral vector or lentiviral vectors carrying ETV2 construct, as in the *in vitro* cell culture. Subsequently, the cells were resuspended in 50 μl PBS mixed with Matrigel (Corning, 356237) or a matrix (containing laminin, entactin, and type-IV collagen) to a total volume of 350 μl, 10 ng/ml FGF2 (Peprotech, 1000–18B), 20 ng/ml VEGF-A (Peprotech, 100–20), and 100 μg/ml heparin (Sigma H3149–100KU). The cells (approximately 2 million per plug), labeled with GFP or mCherry, were injected subcutaneously into 8- to 12-week-old SCID-beige mice (Taconic). Each mouse received two plugs – one containing control HUVECs and one containing *Etv2*$^+$ HUVECs. The plugs were present in each mouse for four different periods – 1 week, 1 month, 2 months, and 5 months. Following their post-euthanasia removal at each time point, whole-mount image stacks were taken of the whole plugs using a Zeiss 710 confocal microscope.

Western blots were obtained for proteins indicative of normal cellular function, as well as to determine the effects of *Etv2* expression *in vivo*; these proteins included Rap1-GTP (active Rap1), GAPDH, VEGFR-2, FLI1, and Etv2.

Fluorescence images were obtained using a Zeiss 710 confocal microscope, to determine relative changes in expression of podocalyxin, actin, VECAD, and Etv2 in *Etv2*$^+$ HUVECs as compared to control HUVECs.

Image processing and vessel morphological analysis

All vascular bed images were first converted from Zeiss LSM z-stacks into high-resolution layer-by-layer images using the built-in converter in the ZEN Blue Edition 2012 software package (Carl Zeiss Microscopy, Germany) (Cunha et al., 2016). Subsequently, these images were exported to ImageJ (National Institutes of Health, USA), where the ‘Split Channels’ tool was used to remove all non-vessel pixels corresponding to nuclear stains and other noise (*in vitro*, Fig. 1b; *in vivo*, Fig. 1f). Afterward, within Adobe Photoshop CS6, the unsharp mask filter with a radius of 12 pixels was applied to intensify the vascular bed while minimizing the background noise (Gould et al., 2011; Kimori, 2011).

Further analysis was performed using ImageJ and the plug-in FracLac for ImageJ (Karperien A, version 2.5) (Cavallari et al., 2011). Using ImageJ, the images were converted from their original 8-bit color to binarized images (*in vitro*, Fig. 1c; *in vivo*, Fig. 1g), due to FracLac and most two-dimensional fractal analysis tools requiring the use of two-color images (de Souza Lins Borba et al., 2016; Gould et al., 2011). The vessels themselves remained white, while the background and other noise were black. FracLac was used to determine the fractal dimension and lacunarity of each image.

Fractal analysis of each vessel was performed using a typical box-counting method, with a grid of known box dimension r (the scale) being overlaid on each image. The number of grid boxes containing white (non-zero) pixels, N_r, was counted (*in vitro*, Fig. 1d; *in vivo*, Fig.

1h). This box-counting procedure was repeated for 100 grids of varying r, with the number of boxes containing non-zero pixels of interest decreasing exponentially as r increased. A mean fractal dimension, D, was calculated in FracLac via the generation of a log-log plot of r versus N_r (*in vitro*, Fig. 1e; *in vivo*, Fig. 1i), with D corresponding to the negation of the slope of the linear regression line applied to this plot (Captur et al., 2013). Additionally, D was calculated at each scale and averaged, as a quality control tool for the regression calculation of D. In this analysis, 12 arbitrary box sizes in the range of 5 to 300 pixels were used for each image. Skeletonization, a method commonly used to isolate the vessel outline, was not used in order to preserve intensity differences and other variations present in the stained vessel network.

Lacunarity was also measured using an overlaid grid, but in this case a sliding box scan algorithm was used (Zudaire et al., 2011). This method involves sliding boxes over the image in an overlapping pattern. This method is preferable to a fixed box scan, where a fixed grid of boxes is applied to the image, since the sliding box scan is more sensitive to subtle non-zero pixel density variations in small regions. The mean and standard deviation (μ and σ, respectively) of pixels per box was calculated for each box size r, and Λ was calculated using Equation 3. Subsequently, an average lacunarity was calculated from the individual lacunarity values at each box size.

The above analytical process was performed for control HUVECs and *Etv2*$^+$ HUVECs, each at 1 week, 1 month, 2 month, and 5 month time points. Thus, mean D and Λ values were found for each of those groups. Additionally, D and Λ were calculated for two known patterns, a straight line and a checkerboard, to validate the methods used and normalize the results if required. Statistical differences in D and Λ were tested using a two-tailed t-test with a 95% confidence interval.

This process of calculating D and Λ was repeated for several distinct *in vitro* and *in vivo* EC vessel beds, created as described above. To investigate the temporal stability of *Etv2*$^+$ cells *in vivo*, HUVECs were studied *in vivo* with and without *Etv2* upregulated at 1 week, 1 month, 2 month, and 5 month time points. Additionally, *Etv2*$^+$ and *Etv2*$^-$ HUVECs *in vivo* were studied in co-culture with colon tumor organoids after 5 months. In terms of *in vitro* studies, *Etv2*$^+$ HUVECs were grown in parallel co-cultures with normal colon organoids and with colon tumor organoids, and *Etv2*$^+$ and *Etv2*$^-$ HUVECs were grown on their own.

To further characterize cell morphology, HUVECs and *Etv2*$^+$ HUVECs were seeded onto individual 35 mm four-chamber glass bottom dishes (Cellvis D35C4–20-1.5N), with the glass at the bottom of each well having a 20-mm diameter. Both cell types were plated at a density of 2,000 cells per well (an average of 6.37 cells/mm^2). These HUVECs were visualized with transfected LifeAct-mNeonGreen to visualize F-actin without interfering with F-actin dynamics (Chertkova et al., 2020; Riedl et al., 2008). Images of the plated cells were taken immediately after plating, and every five minutes thereafter for a total of 250 minutes. The diameters of ten random F-actin fibers were measured in each image.

AFM Measurements

AFM was used to examine the morphology and stiffness of live HUVECs and adult adipose ECs, with AFM of live ECs being relatively common (Stroka and Aranda-Espinoza, 2011; Vargas-Pinto et al., 2013; Okamoto et al., 2017). To determine target locations for stiffness measurements, brightfield images of cells were acquired using an inverted microscope (Zeiss Axio Observer Z1) as the AFM base (20× 0.8 NA objective). An MFP-3D-BIO Atomic Force Microscope (Asylum Research) was used to collect force versus indentation curves at various locations across each sample, under fluidic condition and a controlled temperature of 37°C. A 5 μm spherical borosilicate glass beaded probe (Novascan) with a nominal spring constant of 0.12 N/m was used for all measurements. The probe was calibrated using the thermal tune method (te Riet et al., 2011). The trigger point was set to 0.2 nN with an approach velocity of 5 μm/sec. A representative force (F) versus indentation (δ) curve was created for a control HUVEC cell (Supplementary Fig. 1). The force-indentation curves were fitted to the Hertz model for spherical tips using

$$F = \frac{4ER^{0.5}}{3\left(1-\upsilon^2\right)}\delta^{1.5}, \tag{4}$$

where the Young's modulus of the cell (E) is the only fitting parameter, R is the radius of the spherical probe, and υ is the Poisson's ratio of the cell which is assumed to be 0.45 (Chen et al., 1996; Lee et al., 2018; Cárdenas-Pérez et al., 2018).

Force maps were created using grids of 20 × 20 grid force curves (400 force curves total), which covered an area of 360 μm^2. Force maps of stiffness along with individual stiffness values for each measured point were exported for further analysis. A custom MATLAB (MathWorks) script was written to accurately analyze the data for cell stiffness and to filter measurements such that only data 1 μm above the glass bottom dish was analyzed to remove any substrate effect. To validate the findings from AFM using the spherical probe, AFM was repeated with a pyramidal borosilicate probe with radius of 42 ± 12 nm and a nominal spring constant of 0.09 N/m.

This testing process was performed on the control adult adipose tissue ECs and HUVECs, to determine whether the observed effects of *Etv2*$^+$ upregulation on stiffness are similar in young ECs isolated from an umbilical cord and relatively older ECs isolated from an older adult. In addition, HUVECs were tested using AFM after exposure to Rap1, a regulatory inhibitor with a role in angiogenesis, among other processes (Carmona et al., 2009).

Results

Etv2$^+$ *HUVECs form complex, homogeneous, and stable vessels in vitro and in vivo* Among ECs cultured *in vitro* (Fig. 2a-c), D was significantly lower for the co-culture of normal colon tissue with *Etv2*$^+$ HUVECs than for *Etv2*$^+$ HUVECs alone ($p = 0.0151$), and D was significantly greater than for control HUVECs alone (p = 0.0015). Among these same two *Etv2*$^+$ systems, $\wedge$ was not significantly different between *Etv2*$^+$ HUVECs and the normal colon co-culture (p = 0.0981). The insignificant difference in $\wedge$ between *Etv2*$^+$ HUVECs and the normal co-culture suggests that the role of the *Etv2*$^+$ HUVECs in the co-culture is

substantial compared to that of the normal colon organoid. Furthermore, in the co-culture *Etv2* dictates D while epithelial cells drive $\curlywedge$ due to vessels preferentially building around the organoids. When colon tumor organoids were co-cultured with $Etv2^+$ HUVECs, D was higher than for $Etv2^+$ HUVECs alone ($p = 0.0184$); however, lacunarity was also higher in the tumor co-culture ($p = 0.0028$).

For HUVECs grown *in vivo* in tissue plugs at 5 months of growth (Fig. 3a-c), D was not significantly different between colon tumor organoid co-cultured with $Etv2^+$ HUVECs than for colon tumor organoid co-cultured with control HUVECs ($p = 0.3743$). Additionally, tumor tissue with $Etv2^+$ HUVECs had a significantly lower $\curlywedge$ than both tumor tissue with control HUVECs ($p < 0.0001$) and tumor tissue with $Etv2^+$ HUVECs ($p < 0.0001$). $Etv2^+$ HUVECs did not have a significantly different D than that of control HUVECs co-cultured with colon tumor organoid.

D and $\curlywedge$ were used to determine if it is possible to quantify EC stability over time. HUVECs grown *in vivo* in tissue plugs (Fig. 4a-c) were analyzed at various time points (1 week, 1 month, 2 months, and 5 months) to determine an aspect of the stability of transcriptionally modified and control ECs over time. Among $Etv2^+$ HUVECs, D was always significantly greater than for control HUVECs ($p < 0.0001$ at all four time points), and $Etv2^+$ HUVECs remained within 7.7% of the original value of D (Supplementary Video 1) while control HUVECs had a D at 2 months that was 25.0% lower than the original D. In terms of $\curlywedge$, $Etv2^+$ consistently had $\curlywedge$ lower than control HUVECs ($p < 0.0001$ at the four time points). Additionally, $\curlywedge$ fluctuated by approximately 26.5% for $Etv2^+$ HUVECs (Supplementary Video 1), while the fluctuation was 40.0% for control HUVECs. In both $Etv2^+$ and control HUVECs, there was a significant drop in both D and $\curlywedge$ between 1 week and 1 month. Overall, Etv2 expression correlates with a greater D and lower $\curlywedge$, with both parameters remaining more stable over time compared to control cells.

Etv2$^+$ *HUVECs form softer vessels*

AFM testing was conducted to measure the stiffness of HUVECs (controls and $Etv2^+$), these same HUVECs exposed to the regulatory inhibitor Rap1 in DMSO, and adult adipose tissue ECs (controls and $Etv2^+$). First, HUVECs were tested via AFM without Rap1 treatment (Fig. 5a,c). Without inhibitor, control HUVECs had a significantly greater mean stiffness than $Etv2^+$ HUVECs ($p < 0.0001$). Relative to control HUVECs, Rap1-GEF expression was upregulated in $Etv2^+$ HUVECS, resulting in higher levels of Rap1 activity as demonstrated by elevated levels of Rap1-GTP (Fig. 5b).

Upon exposure to Rap1, the difference in mean stiffness for control and $Etv2^+$ HUVECs was insignificant ($p = 0.0500$). To confirm that DMSO treatment did not play a role in reduction of stiffness, control and $Etv2^+$ HUVECs were exposed to DMSO in the absence of Rap1. The difference in stiffness between control & $Etv2^+$ HUVECs in this case remained significant ($p < 0.0001$).

To demonstrate stiffness of an applicable treatment group, adult adipose ECs (both control and $Etv2^+$ samples) were also tested. For each test of an EC by AFM, a stiffness map was generated (Fig. 6a-d) to demonstrate how stiffness changed with position of the spherical

AFM probe on the cell surface. These maps help visualize the stiffness measurements in the spatial context of the cell, using a spherical probe (Fig. 6e) and a pyramidal probe (Supplementary Fig. 2). As was the case for HUVECs, control adult ECs were significantly stiffer than *Etv2*$^+$ adult ECs, regardless of probe shape ($p < 0.0001$). The control adipose ECs were significantly stiffer than control HUVECs, while the stiffness of *Etv2*$^+$ adipose ECs was not significantly different from that of their HUVEC counterparts.

Further characterization of Etv2$^+$ *HUVECs verifies their improved mechanical integrity*

Additional staining with fluorescent markers was conducted to elucidate the effects that upregulated expression of Etv2 protein had on the mechanical integrity of vessel structures (Fig. 7a). Podocalyxin levels were not significantly different in *Etv2*$^+$ HUVECS compared to controls. The expression of F-actin and VECAD was substantially higher in *Etv2*$^+$ HUVECs compared to control HUVECs.

Western blots were used to validate *Etv2* upregulation in HUVECs, and to confirm the absence of Etv2 in control HUVECs treated with an empty vector (Fig. 7b). Etv2 expression was prominent in *Etv2*$^+$ HUVECs and effectively undetectable in controls. VEGFR-2 expression was also elevated in *Etv2*$^+$ HUVECs.

To further characterize the F-actin using traditional measures, fiber diameters were measured at 25-minute intervals after cell plating, for control HUVECs and *Etv2*$^+$ HUVECs. Compared to their starting diameter, the F-actin fibers decreased in diameter significantly less in *Etv2*$^+$ HUVECs (about 7.3%) compared to in control HUVECs (about 28.4%). Additionally, *Etv2*$^+$ HUVEC F-actin diameter rebounded quickly (within 25 minutes) following the initial drop in diameter, while control HUVEC F-actin diameter precipitously declined.

Discussion

Growth of tissues *in vitro* for transplantation into humans is a promising area of research, with potential uses in diseased and severely injured tissues. However, vascularization of these tissue constructs using various growth factors does not have sufficiently proven temporal stability or mechanical integrity for high-shear flow found in many native vessels that may need to be replaced by this transplant. We have demonstrated that fractal analysis and AFM testing of vessels provides reproducible quantitative information regarding vessel stability, as well as the utility of *Etv2* upregulation in enhancement of vascularization.

ECs expressing Etv2 *form vessels favorable for tissue constructs*

There was a higher D and lower Λ for *Etv2*$^+$ HUVECs when compared to control HUVECs, both *in vitro*. The higher D indicates a greater complexity and greater space-filling properties, which in the case of vasculature means there was more branching and greater vessel density when *Etv2* was upregulated. This is beneficial because the development of a higher vessel density within the same time period will allow for higher viability of transplanted tissue constructs due to more organ-wide vascularization. The decrease in Λ with induction of *Etv2* indicates an increased structural homogeneity (i.e., more homogeneous vessel spacing and branching points); this means that the branching points

are more predictable when *Etv2* is upregulated. It is essential to ensure that the ECs used are mostly *Etv2*$^+$, because the co-culture of control and *Etv2*$^+$ HUVECs led to a significant increase in Λ compared to *Etv2*$^+$ HUVECs alone. Lower Λ values observed in *Etv2*$^+$ HUVECs are favorable in blood vessel organization because of the reliable vessel spacing, which ensures that the presence of non-vascularized tissue sectors is minimized.

The *in vitro* co-culture of colon tumor organoid with *Etv2*$^+$ HUVECs led to a significant increase in Λ compared to *Etv2*$^+$ HUVECs alone. The higher Λ generally seen in vessels in various tumor types *in vivo* explains this increase in Λ; thus, the tumor organoids played a substantial role in determining lacunarity. The fractal dimension in *Etv2*$^+$ HUVECs with colon tumor tissue was significantly more variable than that of *Etv2*$^+$ HUVECs grown alone *in vivo*; this indicates that tumor ECs generally have a more consistent D than non-tumor cells. Additionally, the tumor vessels had a higher lacunarity than the normal vessels, which means that the tumor vessels were more heterogeneously spaced and the branching was less regular. This is in agreement with perceived dysfunctional tumor vasculature, given that tumor vessels grow rapidly but not necessarily in physiologically pre-determined patterns. One review noted the irregular, leaky, and tortuous courses in vessels found in cancers and other angiogenic disorders (Carmeliet and Jain, 2011), and a different group described the unorganized, tortuous appearance of vessels in a variety of tumors (McDonald and Choyke, 2003).

In vivo, *Etv2*$^+$ vessels always had a higher fractal dimension and lower lacunarity than control vessels over a five-month period. Upregulation of *Etv2* therefore leads to denser, more homogenous, and comparatively properly patterned stable vessel growth *in vivo*. Once the method for *Etv2* upregulation becomes more efficient, it has the promise for increasing and normalizing vasculogenesis and angiogenesis both *in vitro* and *in vivo*.

Etv2 enhances vessel stability

While a general increase in fractal dimension and decrease in lacunarity in Etv2-transduced cells is promising, the most immediately applicable finding is that *Etv2*$^+$ HUVECs produce vessels more readily and stably.

Etv2$^+$ vessels grown *in vivo* in a tissue plug in the colon of mice were significantly denser (as indicated by their higher fractal dimension) and more homogeneous (as indicated by their lower lacunarity) than control vessels. This was true at several time points including 1 week, 1 month, 2 months, and 5 months. The smaller percent fluctuation in D over time for *Etv2*$^+$ HUVECs demonstrates that vessels grown with such transcriptional modification will help tissue remain viable until its vasculature and connective tissue is fully integrated into a patient's organ and tissue systems. Additionally, the higher Λ in the control vessels implies that they are more randomly spaced and irregularly grouped than *Etv2*$^+$ vessels.

In addition to temporal stability, *Etv2*$^+$ HUVECs more easily form cylindrical vessels *in vitro* due to their lower stiffness compared to that of control cells. This was shown using AFM testing of stiffness for both adult ECs and HUVECs. The stiffness (Young's modulus) values for live control HUVECs measured in this study were comparable to previously published data for live and fixed HUVECs (Oberleithner et al., 2006; Stroka and Aranda-

Espinoza, 2011). Since the stiffness difference between control and *Etv2*$^{+}$ HUVECs is comparable for adult and umbilical (i.e., younger) tissues, the applicability of the fractal analysis of HUVECs (with and without adult tissue present in culture) is clearer and nearly direct.

A mechanistic explanation for the enhanced vessel stability in *Etv2*$^{+}$ HUVECs resulted from the comparative inspection of key protein levels in *Etv2*$^{+}$ and control cells. Podocalyxin has a key role in the formation of vascular lumens (with podocalyxin staining apical regions of the vessel) and regulation of vascular permeability (Cait et al., 2019). Levels of actin and vascular endothelial cadherin (VECAD) were used to elucidate some of the structural protein-based mechanisms enhancing vessel integrity in *Etv2*$^{+}$ HUVECs. Actin is a multifunctional protein forming microfilaments, and is essential in maintaining cytoskeletal mechanical integrity and in the formation of robust cell-cell junctions in vascular endothelium (De La Cruz and Gardel, 2015). VECAD is also important in vascular endothelial junctions. Both actin and VECAD play regulatory roles in angiogenesis (Cao et al., 2017).

Substantially elevated actin accompanied by overexpressed VECAD and VEGFR-2 explains in part the temporal stability of *Etv2*$^{+}$ vasculature *in vivo* – VEGFR-2/Notch signaling is important in the induction of angiogenic growth, while VECAD and actin are key in regulation of angiogenesis and maintenance of vessel integrity during circulation *in vivo*. Furthermore, the substantial rebound and subsequent maintenance of F-actin diameter in *Etv2*$^{+}$ HUVECs, when compared to control HUVECs, indicated repair and reinforcement of the F-actin fibers over time, rather than the weakening of these fibers observed in control HUVECs. This enhanced F-actin diameter, alongside an initial decrease in cell and vessel stiffness, likely plays a role in enabling successful vessel cylindrification and ingrowth by *Etv2*$^{+}$ HUVECs.

A further mechanistic insight is that Etv2-induced expression of Rap1 equalized the stiffnesses of control and *Etv2*$^{+}$ HUVECs, suggesting that the beneficial effects of *Etv2* (in terms of an initial decrease in vessel stiffness) are tied to one or more regulatory proteins or pathways inhibited by Rap1.

Fractal mathematics is important when analyzing vascular growth in vivo and in vitro

For both *in vitro* and *in vivo* culture, fractal dimension and lacunarity were useful in parallel to identify parameters including degree of vessel branching, homogeneity of vessel diameter and location, and the effective density of vessels capable of perfusion (i.e., vessels part of a continuous network rather than an isolated vessel group). Simple unifractal analysis can be applied to any two-dimensional image that can be binarized without loss of vital information, and thus has applications for all vessel beds that can be imaged. Examples of such applications include the longitudinal study of vessel remodeling following brain trauma, the quantification of vessel properties for postoperative and postmortem analysis tissue grafts used in mouse and human studies, and a supplemental differential diagnostic criterion for retinal disorders.

In addition to vessels, fractal analysis can be applied to other biological tissues and cultures that exhibit recursive or quasi-recursive growth or shape. Examples of these tissues include the lung airway, trabeculae of bone, and neurons. Additionally, dynamic processes often exhibit fractal behavior and timing. For example, in addition to its periodic nature, the heartbeat is slightly fractal when examined in fine detail (especially regarding minute fluctuations in the heart rate), and thus there is potential for detecting various cardiovascular disease signs with tools that include fractal analysis. Specifically, the changes in intervals between heartbeats are not independent, with instantaneous adjustments in rate taking on a scale-invariant (i.e., fractal) pattern at multiple timescales (Pittman-Polletta et al., 2013).

The most immediate use of the tools utilized in this study is in vascularization efforts in the development of viable transplantable tissue constructs. We identified and verified the improved strength and stability in *Etv2*$^{+}$ HUVEC vasculature through quantitative analysis of vessel images (fractal dimension and lacunarity), protein studies, and AFM. The presence of greater branching, vessel density, and elasticity of *Etv2*$^{+}$ HUVECs is conducive to the formation of self-organizing vessels with durable lumens and subsequently an adaptive vascular niche which forms perfusable vascular plexi. Leveraging *Etv2* upregulation to mimic in tissue and organ constructs the stable and rapid growth of vessels typically found in embryos, we are perhaps one step closer to using such tissues successfully and reliably.

Supplementary Material

Refer to Web version on PubMed Central for supplementary material.

Acknowledgments

S.Y.R. is supported by the Cell and Tissue Engineering Program at Hofstra Univerity. S.R. is supported by the Ansary Stem Cell Institute; grants from the National Institutes of Health (NIH) (R35 HL150809, R01s DK095039, HL119872, HL128158, HL115128, HL139056, RC2DK114777 and U01AI138329); the Empire State Stem Cell Board; grants from New York State Stem Cell Science (NYSTEM) (C025878, C028117, C029156, C030160); and the Starr Foundation stem cell core project. We thank Matthew Brendel from Memorial Sloan Kettering Cancer Center for input regarding methodology and Duc-Huy T. Nguyen from Weill Cornell Medicine for experimental data.

Appendix

Author Contributions (CRediT roles)

Morphological Characterization of *Etv2* Explants Using Fractal Analysis and Atomic Force Microscopy

Robert P. Adelson: Methodology, Software, Validation, Formal analysis, Writing - Original Draft, Writing - Review & Editing, Visualization. **Brisa Palikuqi:** Conceptualization, Methodology, Validation, Formal analysis, Investigation, Data Curation, Writing - Review & Editing, Project administration. **Zachary Weiss:** Methodology, Software. **Antonio Checco:** Validation, Investigation, Data Curation. **Ryan Schreiner:** Methodology, Software, Formal analysis, Writing - Review & Editing. **Shahin Rafii:** Conceptualization, Methodology, Resources, Writing - Review & Editing, Supervision, Project administration, Funding acquisition. **Sina Y. Rabbany:** Conceptualization, Methodology, Validation, Investigation,

Resources, Writing - Original Draft, Visualization, Supervision, Project administration, Funding acquisition.

Disclosure Statement

S.R. is the founder and a non-paid consultant to Angiocrine Bioscience.

Ethics Declaration

Experiments utilizing the following animals were performed under the approval of the Weill Cornell Medicine Institutional Animal Care and Use Committee (IACUC), New York, NY):

- SCID Beige mice (male and female, 8–12 weeks old) from Taconic were used for implants.
- ETV2 reporter mice were a kind gift from Dr. Valerie Kouskoff. Embryos from E9.5 pregnant female ETV2/+ reporter mice were used to isolate endothelial cells with or without ETV2 expression. Only embryos positive for ETV2 reporter were used.

HUVECs were isolated from human umbilical cords obtained as left-over discarded tissues at the New York Presbyterian Hospital. The population is healthy full-term pregnant women who have either undergone Caesarian section or normal delivery. Fat endothelial cells were isolated from human fat tissue obtained from leftover tissue after reconstructive surgery at the New York Presbyterian Hospital. The population is health adult individuals. Normal and adenoma tissues were collected from colonic restrictions.

The IRB at Weill Cornell Medicine deemed the studies on HUVECs exempt from the requirement of informed consent. As umbilical cords are deemed discarded tissues, the recruitment does not require informed consent and is obtained through the hospital personnel depending on the availability of the discarded and left-over umbilical cords. Fat endothelial cells and normal and adenoma tissues from colonic resection were collected according to protocols approved by the Weill Cornell Medicine Institutional Review Board (IRB) following appropriate consent.

Availability of Data and Material

The datasets used and/or analyzed during the current study are available from the corresponding author upon reasonable request.

References

Baltrunaite K, et al., 2017. ETS transcription factors Etv2 and Fli1b are required for tumor angiogenesis. Angiogenesis. 20, 307–323. [PubMed: 28108843]

Cait J, et al., 2019. Podocalyxin is required for maintaining blood-brain barrier function during acute inflammation. PNAS. 116, 4518–27. [PubMed: 30787191]

Cao J, et al., 2017. Polarized actin and VE-cadherin dynamics regulate junctional remodelling and cell migration during sprouting angiogenesis. Nat Commun. 8, 2210. [PubMed: 29263363]

Captur G, et al., 2013. Quantification of left ventricular trabeculae using fractal analysis. J Cardiovasc Magn Reson. 15, 36. [PubMed: 23663522]

Cárdenas-Pérez, et al., 2018. Recent advances in atomic force microscopy for assessing the nanomechanical properties of food materials. Trends Food Sci Technol. 87, 59–72.

Carmeliet P, Jain RK, 2011. Principles and mechanisms of vessel normalization for cancer and other angiogenic diseases. Nat Rev Drug Discov. 10, 417–27. [PubMed: 21629292]

Carmona G, et al., 2009. Role of the small GTPase Rap1 for integrin activity regulation in endothelial cells and angiogenesis. Blood. 113, 488–97. [PubMed: 18805968]

Cavallari M, et al., 2011. Fractal analysis reveals reduced complexity of retinal vessels in CADASIL. PLoS One. 6, e19150. [PubMed: 21556373]

Chen EJ, et al., 1996. Young's modulus measurements of soft tissues with application to elasticity imaging. IEEE Transactions on Ultrasonics, Ferroelectrics, and Frequency Control. 43, 191–194.

Chertkova AO, et al., 2020. Robust and Bright Genetically Encoded Fluorescent Markers for Highlighting Structures and Compartments in Mammalian Cells. bioRxiv.

Cunha C, et al., 2016. Exploring New Inflammatory Biomarkers and Pathways during LPS-Induced M1 Polarization. Mediators Inflamm. 2016, 6986175. [PubMed: 28096568]

De La Cruz EM, Gardel ML, 2015. Actin Mechanics and Fragmentation. J Biol Chem. 290, 17137–44. [PubMed: 25957404]

de Souza Lins Borba FK, et al., 2016. Fractal analysis of extra-embryonic vessels of chick embryos under the effect of glucosamine and chondroitin sulfates. Microvasc Res. 105, 114–8. [PubMed: 26873109]

Ding MH, et al., 2020. The Role of Angiogenesis-Inducing microRNAs in Vascular Tissue Engineering. Tissue Eng Part A.

Dufrêne YF, et al., 2017. Imaging modes of atomic force microscopy for application in molecular and cell biology. Nat Nanotechnol. 12, 295–307. [PubMed: 28383040]

Essay M, Maina JN, 2020. Fractal analysis of concurrently prepared latex rubber casts of the bronchial and vascular systems of the human lung. Open Biol. 10, 190249. [PubMed: 32634372]

Frye M, et al., 2018. Matrix stiffness controls lymphatic vessel formation through regulation of a GATA2-dependent transcriptional program. Nat Commun. 9, 1511. [PubMed: 29666442]

Gadde SG, et al., 2016. Quantification of Vessel Density in Retinal Optical Coherence Tomography Angiography Images Using Local Fractal Dimension. Invest Ophthalmol Vis Sci. 57, 246–52. [PubMed: 26803800]

Gould DJ, et al., 2011. Multifractal and lacunarity analysis of microvascular morphology and remodeling. Microcirculation. 18, 136–51. [PubMed: 21166933]

Haase K, Pelling AE, 2015. Investigating cell mechanics with atomic force microscopy. J R Soc Interface. 12, 20140970. [PubMed: 25589563]

Kant RJ, Coulombe KLK, 2018. Integrated approaches to spatiotemporally directing angiogenesis in host and engineered tissues. Acta Biomater. 69, 42–62. [PubMed: 29371132]

Kimori Y, 2011. Mathematical morphology-based approach to the enhancement of morphological features in medical images. J Clin Bioinforma. 1, 33. [PubMed: 22177340]

Lee JJ, et al., 2018. Dehomogenized Elastic Properties of Heterogeneous Layered Materials in AFM Indentation Experiments. Biophys J. 114, 2717–2731. [PubMed: 29874620]

Lennon FE, et al., 2015. Lung cancer-a fractal viewpoint. Nat Rev Clin Oncol. 12, 664–75. [PubMed: 26169924]

Mainster MA, 1990. The fractal properties of retinal vessels: embryological and clinical implications. Eye (Lond). 4 (Pt 1), 235–41. [PubMed: 2323476]

Mastrullo V, et al., 2020. Angiogenesis in Tissue Engineering: As Nature Intended?Front Bioeng Biotechnol. 8, 188. [PubMed: 32266227]

McDonald DM, Choyke PL, 2003. Imaging of angiogenesis: from microscope to clinic. Nat Med. 9, 713–25. [PubMed: 12778170]

Oberleithner H, et al., 2006. Differential action of steroid hormones on human endothelium. J Cell Sci. 119, 1926–32. [PubMed: 16636077]

Okamoto T, et al., 2017. Gap junction-mediated regulation of endothelial cellular stiffness. Sci Rep. 7, 6134. [PubMed: 28733642]

Palikuqi B, et al., 2020. Adaptable haemodynamic endothelial cells for organogenesis and tumorigenesis. Nature. 585, 426–432. [PubMed: 32908310]

Park C, et al., 2016. Injury-Mediated Vascular Regeneration Requires Endothelial ER71/ETV2. Arterioscler Thromb Vasc Biol. 36, 86–96. [PubMed: 26586661]

Pittman-Polletta BR, et al., 2013. The role of the circadian system in fractal neurophysiological control. Biol Rev Camb Philos Soc. 88, 873–94. [PubMed: 23573942]

Plotnick RE, et al., 1996. Lacunarity analysis: A general technique for the analysis of spatial patterns. Phys Rev E Stat Phys Plasmas Fluids Relat Interdiscip Topics. 53, 5461–5468. [PubMed: 9964879]

Riedl J, et al., 2008. Lifeact: a versatile marker to visualize F-actin. Nat Methods. 5, 605–7. [PubMed: 18536722]

Singh BN, et al., 2019. Etv2 transcriptionally regulates Yes1 and promotes cell proliferation during embryogenesis. Sci Rep. 9, 9736. [PubMed: 31278282]

Stroka KM, Aranda-Espinoza H, 2011. Endothelial cell substrate stiffness influences neutrophil transmigration via myosin light chain kinase-dependent cell contraction. Blood. 118, 1632–40. [PubMed: 21652678]

Ţălu S, 2013. Characterization of retinal vessel networks in human retinal imagery using quantitative descriptors. Human and Veterinary Medicine5, 52–57.

Ţălu S, 2015. Micro and Nanoscale Characterization of Three Dimensional Surfaces: Basics and Applications. Napoca Star Publishing House: Cluj-Napoca, Romania.

Tanaka T, et al., 2018. ETV2-TET1/TET2 Complexes Induce Endothelial Cell-Specific Robo4 Expression via Promoter Demethylation. Sci Rep. 8, 5653. [PubMed: 29618782]

te Riet J, et al., 2011. Interlaboratory round robin on cantilever calibration for AFM force spectroscopy. Ultramicroscopy. 111, 1659–69. [PubMed: 22094372]

Vargas-Pinto R, et al., 2013. The effect of the endothelial cell cortex on atomic force microscopy measurements. Biophys J. 105, 300–9. [PubMed: 23870251]

von Koch H, 1904. On a continuous curve without tangents, constructible from elementary geometry. Ark Mat Astr Fys. 1, 681–702.

Wang R, et al., 2019. Investigation into the diversity in the fractal dimensions of arterioles and venules in a microvascular network - A quantitative analysis. Microvasc Res. 125, 103882. [PubMed: 31075242]

Zaia A, 2015. Fractal lacunarity of trabecular bone and magnetic resonance imaging: New perspectives for osteoporotic fracture risk assessment. World J Orthop. 6, 221–35. [PubMed: 25793162]

Zhang F, et al., 2003. Green fluorescent protein selectively induces HSP70-mediated upregulation of COX-2 expression in endothelial cells. Blood. 102, 2115–21. [PubMed: 12805066]

Zhao H, et al., 2017. ETS transcription factor ETV2/ER71/Etsrp in hematopoietic and vascular development, injury, and regeneration. Dev Dyn. 246, 318–327. [PubMed: 28026128]

Zudaire E, et al., 2011. A computational tool for quantitative analysis of vascular networks. PLoS One. 6, e27385. [PubMed: 22110636]

Highlights

Morphological Characterization of *Etv2* Explants Using Fractal Analysis and Atomic Force Microscopy

- Methods to analyze vessel fractal dimension (D) and lacunarity (Λ) are presented
- *In vitro* and *in vivo*, *Etv2*$^+$ HUVECs have higher D and lower Λ
- Tumor ECs generally have lower D and higher Λ than non-tumor ECs
- In AFM, live *Etv2*$^+$ HUVECs are less stiff than controls, enabling cylindrification
- *Etv2*$^+$ HUVECs have increased F-actin diameter and overexpress VECAD and VEGFR-2

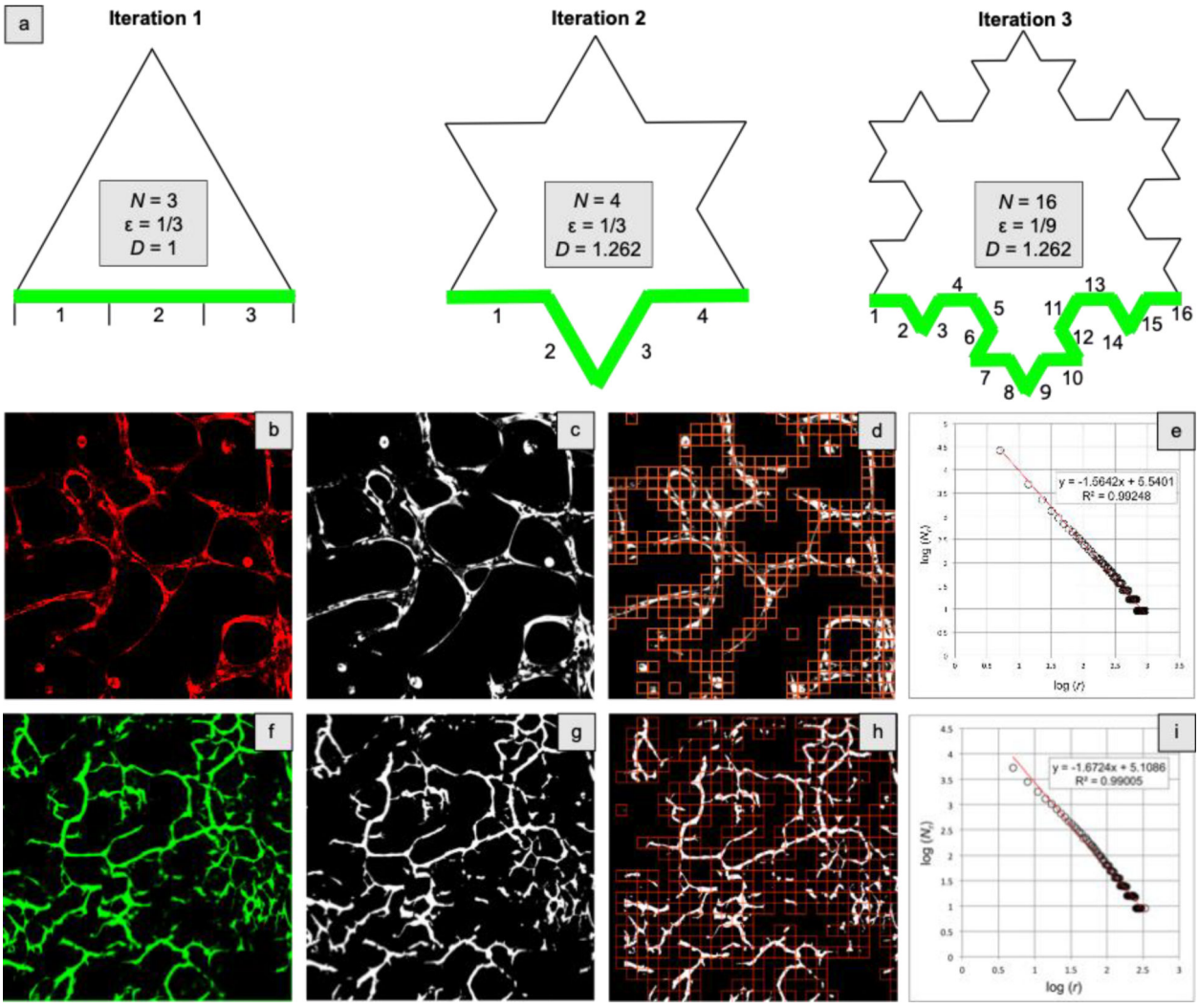

Figure 1. Illustration explaining fractal dimension, and the steps in computing fractal dimension from *in vitro* and *in vivo* vessel networks.

(a) Three steps in the construction of the Koch snowflake. Iteration 1 is an equilateral triangle, where each side is composed of three equal thirds. The fractal dimension (*D*) is 1. Iteration 2 is a hexagram, where each side is composed of four of the segments from iteration 1, making *D* 1.262. In iteration 3, the same process as in iteration 2 is repeated, with each of the four segments from iteration 2 elongated by 1/3; *D* remains 1.262**. (b)** High-resolution layer from a z-stack image file of a healthy *Etv2*$^{+}$ vessel network *in vitro*, following removal of non-vessel pixels using ImageJ. **(c)** The *in vitro* image following binarization in ImageJ. **(d)** In the box-counting method for calculating *D*, a grid of a known *r* scale is overlaid on the *in vitro* image, and the number of boxes containing foreground pixels is counted. **(e)** From various grids as in (d), a log-log plot of *r* versus N_r is generated for the *in vitro* image, and *D* is the additive inverse of the slope of the linear regression line, in this case approximately 1.56. The lacunarity is approximately 0.62. **(f)** High-resolution layer from a z-stack image file of a healthy *Etv2*$^{+}$ vessel network *in vivo*, following removal of non-vessel pixels using ImageJ. **(g)** The same *in vivo* image following binarization in

ImageJ. **(h)** In the box-counting method for calculating D, a grid of a known r scale is overlaid on the *in vivo* image, and the number of boxes containing foreground pixels is counted. **(i)** From various grids as in (h), a log-log plot of r versus N_r is generated for the *in vivo* image, and D is the additive inverse of the slope of the linear regression line, in this case approximately 1.67. The lacunarity is approximately 0.40.

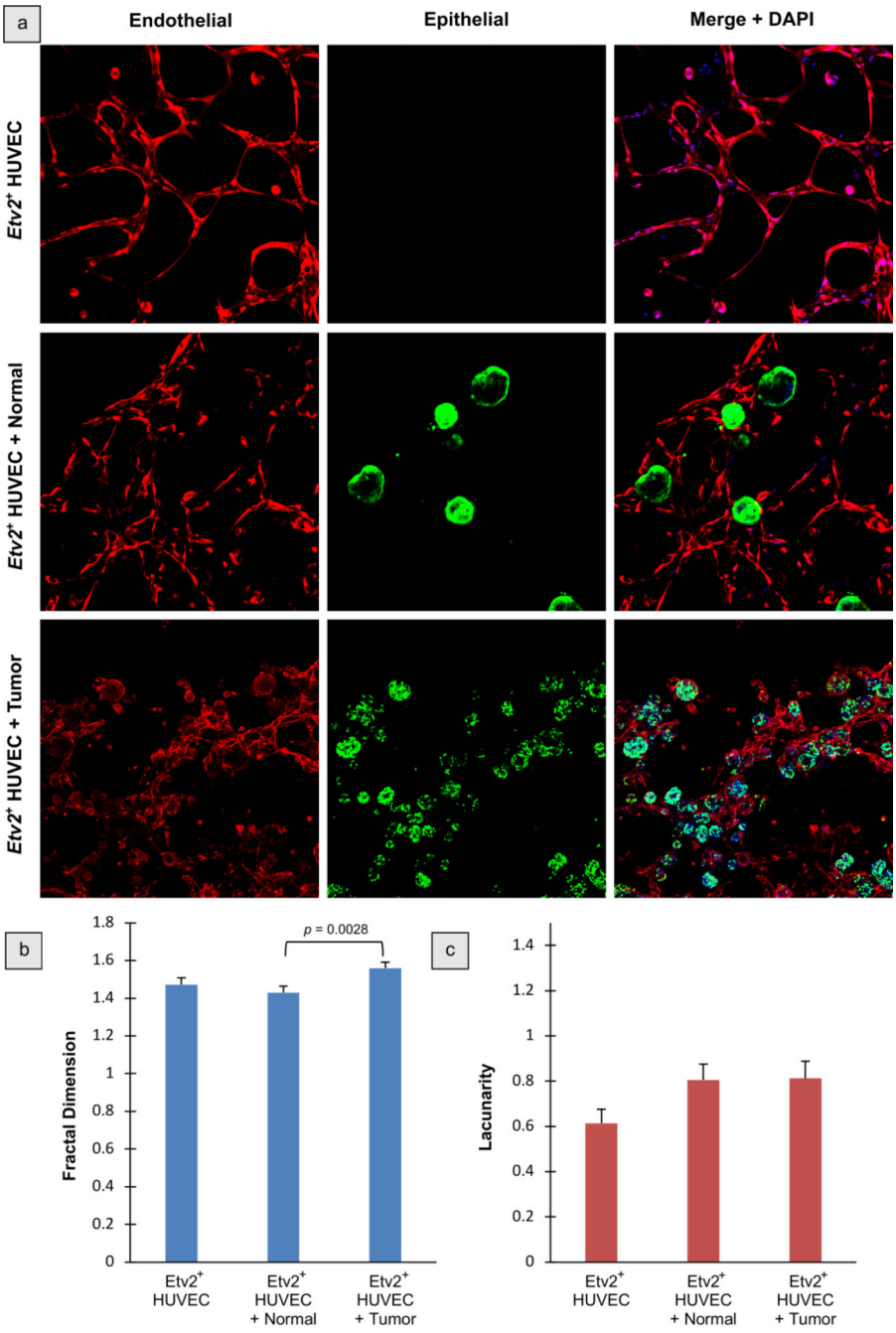

Figure 2. Staining and calculation of fractal dimension and lacunarity *in vitro*.

(a) Stained ECs, epithelial cells, and composite images with DAPI staining, of vessels grown *in vitro* from *Etv2*$^+$ HUVECs, *Etv2*$^+$ HUVECs with normal colon tissue, and *Etv2*$^+$ HUVECs with colon tumor organoids. **(b)** Fractal dimension, and **(c)** lacunarity, for transcriptionally modified (*Etv2*$^+$) HUVECs grown *in vitro*. From left to right in each plot: *Etv2* HUVECs (*Etv2*$^+$ HUVECs cultured alone *in vitro*, $n = 3$ replicates); *Etv2* HUVEC + Normal (the co-culture of normal colon tissue with *Etv2*$^+$ HUVECs, $n = 6$); and *Etv2* HUVEC + Tumor (the co-culture of colon tumor organoids with *Etv2*$^+$ HUVECs, $n =$

6). In each plot, the values are expression as mean ± standard deviation, and statistical differences in fractal dimension and lacunarity were tested using a two-tailed *t*-test with a 99% confidence interval.

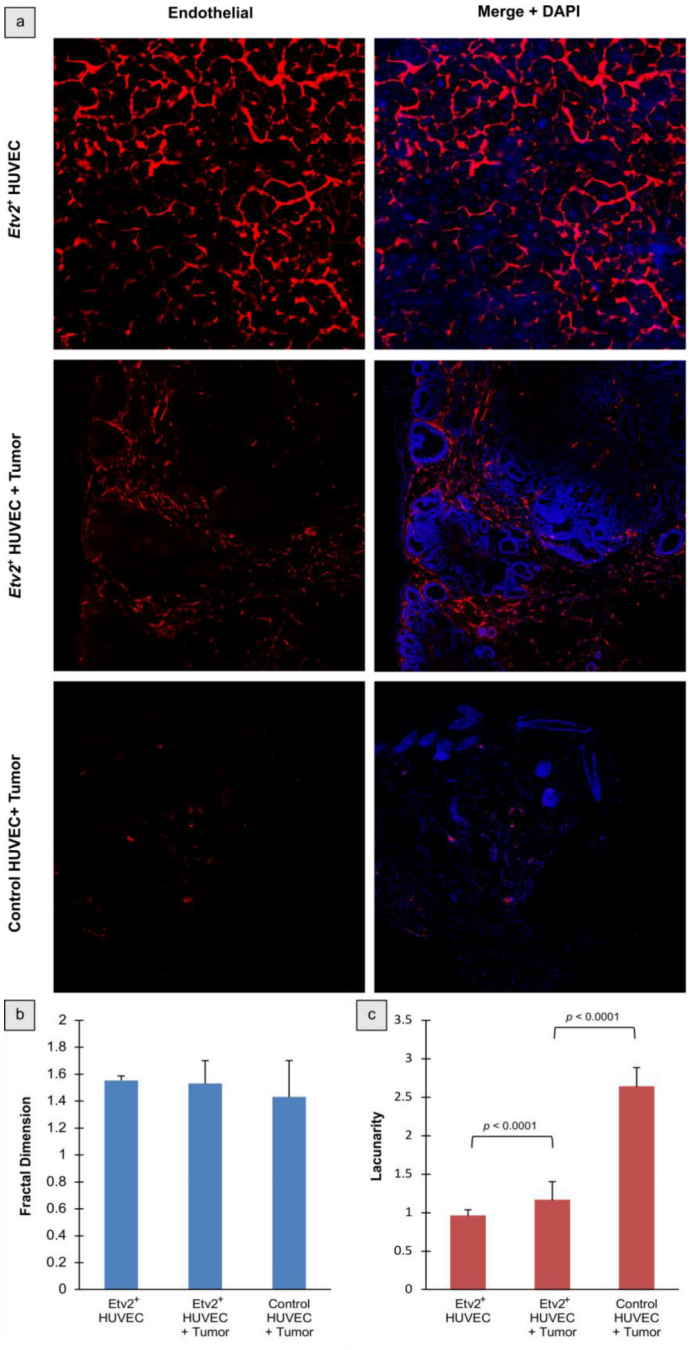

Figure 3. Staining and calculation of fractal dimension and lacunarity *in vivo*.

(a) Stained ECs and composite images with DAPI staining, of vessels grown *in vivo* from *Etv2*$^+$ HUVECs, *Etv2*$^+$ HUVECs with colon tumor organoids, and control HUVECs with colon tumor organoids. **(b)** Fractal dimension, and **(c)** lacunarity, for transcriptionally modified (*Etv2*$^+$) HUVECs grown *in vivo* in a colon tissue plug, following 5 months of growth. From left to right in each plot: *Etv2* HUVEC (*Etv2*$^+$ HUVECs grown without co-culture *in vivo*, $n = 6$); *Etv2*$^+$ HUVEC + Tumor (*Etv2*$^+$ HUVECs grown with colon tumor organoids *in vivo*, $n = 9$); and Control HUVEC + Tumor (normal HUVECs grown with

colon tumor organoids *in vivo*, $n = 8$). In each plot, the values are expression as mean ± standard deviation, and statistical differences in fractal dimension and lacunarity were tested using a two-tailed *t*-test with a 99% confidence interval.

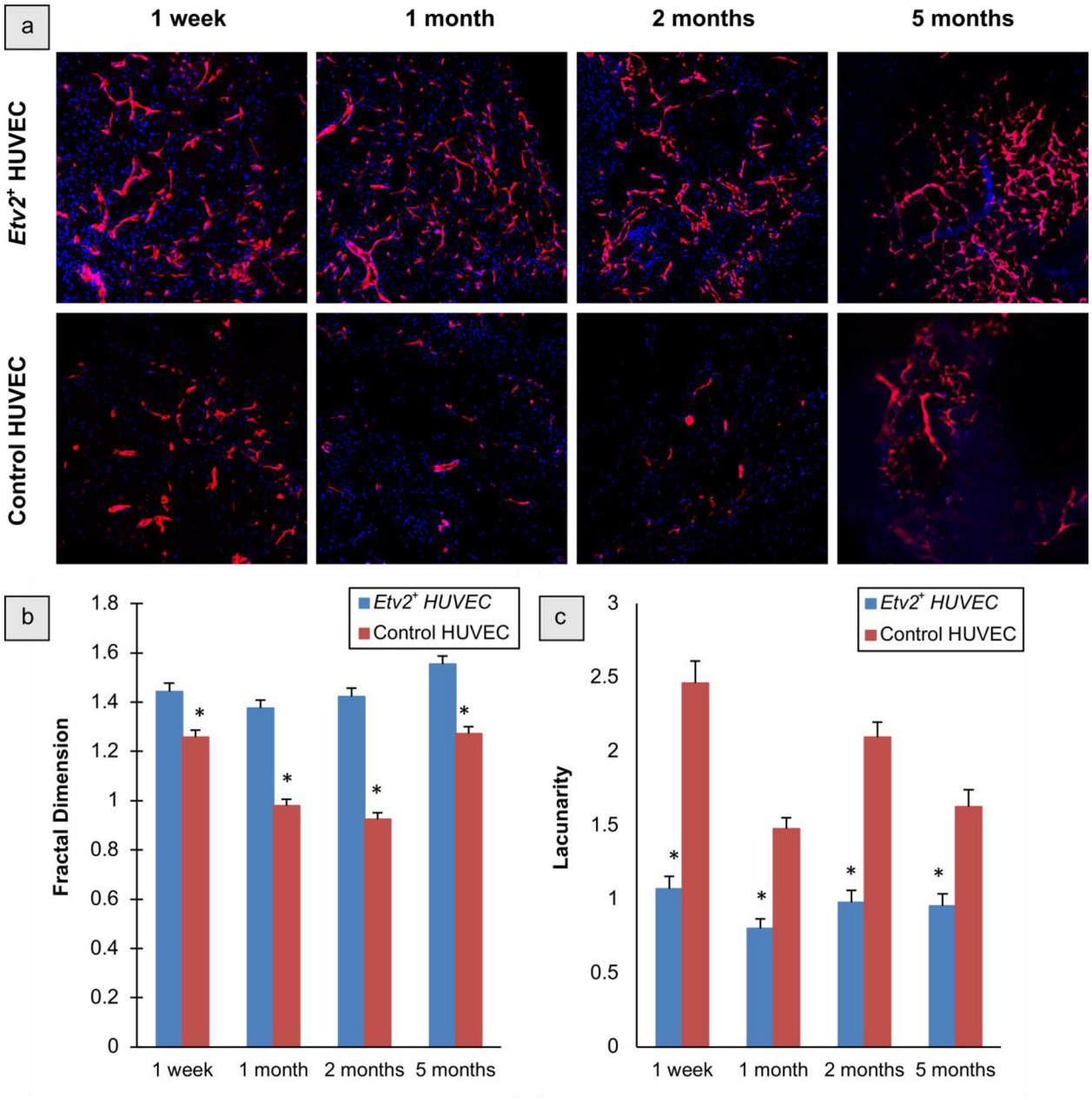

Figure 4. Staining, fractal dimension, and lacunarity over time.

(a) Stained composite z-stack images (ECs and DAPI) of vessels grown *in vivo* from *Etv2*$^+$ HUVECs at time points of 1 week, 1 month, 2 months, and 5 months, and from control HUVECs at the same time points. **(b)** Fractal dimension, and **(c)** lacunarity, for transcriptionally modified (*Etv2*$^+$) and control HUVECs grown *in vivo*, at those four time points. For the *Etv2*$^+$ HUVEC vessels, the time points were: 1 week (n = 18), 1 month (n = 14), 2 months (n = 13), and 5 months (n = 6). For the control HUVEC vessels, the time points were: 1 week (n = 9), 1 month (n = 15), 2 months (n = 13), and 5 months (n = 5). * = Significant at 99% confidence. In each plot, the values are expression as mean ± standard deviation.

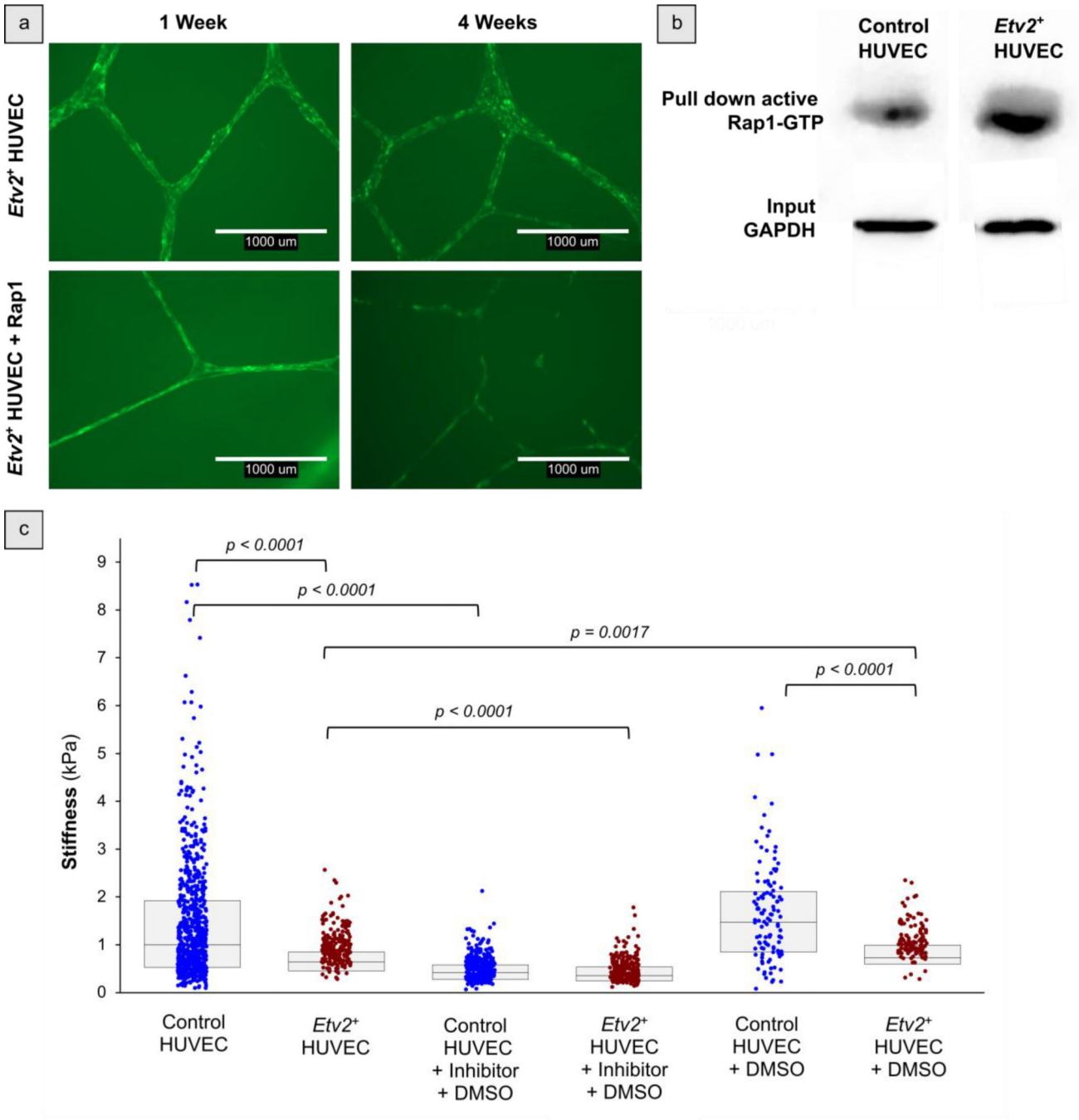

Figure 5. Characterization of vessel networks with and without treatment with Rap1 inhibitor.

(a) Confocal microscopy images of *Etv2*$^+$ vessel networks with and without Rap1 treatment, following 1 week and 1 month of growth following application of Rap1. There was substantial vessel thinning in the presence of Rap1 over time. **(b)** Relative expression levels of Rap1-GTP (the active form) and GAPDH in control (*Etv2*$^-$) and *Etv2*$^+$ HUVECs, as measured by western blot. The upregulation of Rap1-GEFs by Etv2 results in higher levels of Rap1 activity, demonstrated here by elevated levels of Rap1-GTP. GAPDH levels are essentially unchanged. **(c)** Stiffness values as measured by AFM testing of control and

Etv2^{+} HUVECs, each cell type in the presence of a regulatory inhibitor (Rap1) dissolved in DMSO, and each cell type in the presence of DMSO only. Control HUVECs were significantly stiffer than *Etv2*$^{+}$ HUVECs prior to treatment with Rap1. The difference in stiffness between control and *Etv2*$^{+}$ HUVECs was insignificant following treatment with Rap1 in DMSO. The difference in stiffness was significant upon exposure to DMSO on its own, meaning the inhibitor solvent did not differentially affect the stiffness. The abbreviated box plots indicate the interquartile range and median for each condition. Statistical differences in fractal stiffness were tested using a two-tailed *t*-test with a 95% confidence interval.

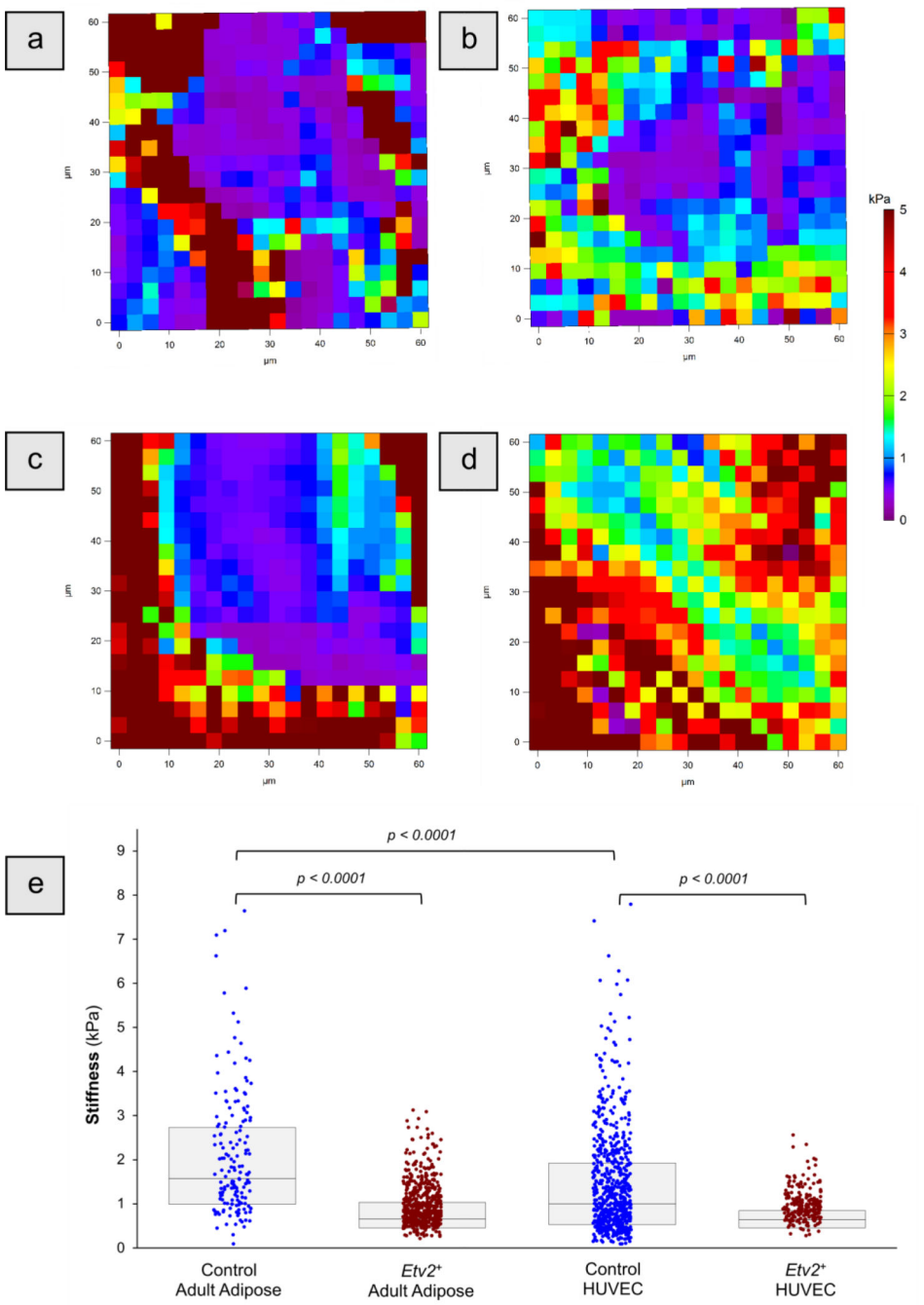

Figure 6. Stiffness values measured by AFM.

The stiffnesses are mapped to position of the AFM probe for **(a)** a control HUVEC, **(b)** an *Etv2*$^{+}$ HUVEC, **(c)** a control adult adipose EC, and **(d)** an *Etv2*$^{+}$ adult adipose EC. Stiffness values measured by AFM testing, **(e)** using a spherical probe of (left to right) adult adipose control ECs, adult adipose *Etv2*$^{+}$ ECs, control HUVECs, and *Etv2*$^{+}$ HUVECs. Control cells were significantly stiffer than *Etv2*$^{+}$ cells for both cell types, demonstrating that Etv2 resets the stiffness of the HUVECs to a younger phenotype. The abbreviated box plots indicate the

interquartile range and median for each condition. Statistical differences in stiffness were tested using a two-tailed *t*-test with a 95% confidence interval.

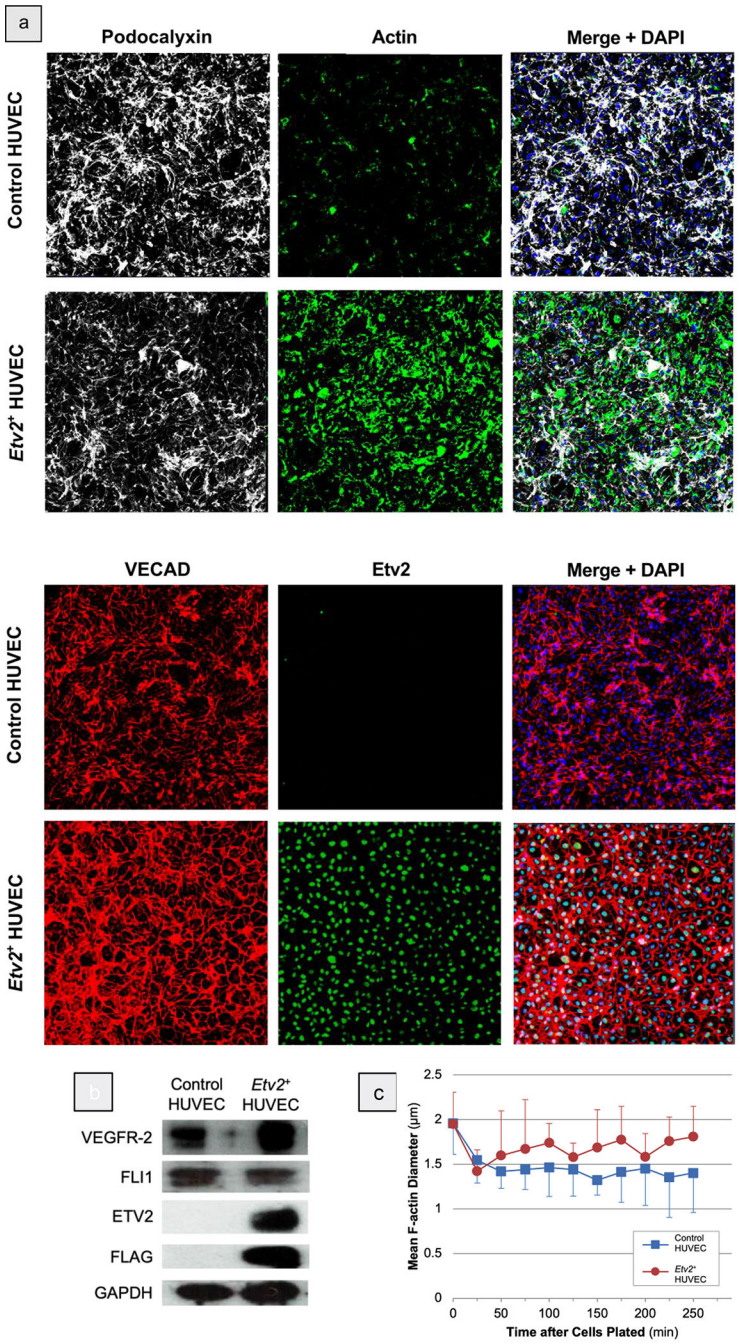

Figure 7. Staining for markers of cell function and stability.

(a) Stained *Etv2*+ HUVECs and control HUVECs, exhibiting the relatively enhanced mechanical properties of *Etv2*+ HUVECS. Podocalyxin levels and distribution appear similar within the two groups. The level of F-actin is considerably higher in *Etv2*+ HUVECs, indicating a more robust network of microfilaments capable of supporting wider vessels with more branch points. Similarly, VE-cadherin (VECAD) levels are enhanced in *Etv2*+ HUVECs, due to the higher concentration of intercellular junctions in these vessel structures. Etv2 protein expression is definitively elevated in *Etv2*+ HUVECS compared to

the controls. **(b)** Relative expression levels of five key proteins (VEGFR-2, FLI1, ETV2, FLAG, GAPDH) in control (*Etv2*$^-$) and *Etv2*$^+$ HUVECs, as measured by western blot. The presence of FLAG and *Etv2* was expected in *Etv2*$^+$ HUVECs. **(c)** Mean F-actin diameter in control HUVECs and *Etv2*$^+$ HUVECs at 25-minute intervals after low-density cell plating. Compared to starting diameter, F-actin fibers decreased in diameter significantly less in *Etv2*$^+$ HUVECs (about 7.28%) compared to in control HUVECs (about 28.37%). Additionally, *Etv2*$^+$ HUVEC F-actin diameter rebounded quickly (within 25 minutes) of the initial drop in diameter. In the plot, the values are expression as mean ± standard deviation.